

Supporting Information

**Lactulose modulation of the Inner Helmholtz Plane for stable and dendrite-free
Zinc anodes in aqueous Zn-ion battery**

Theoretical calculations:

The binding energies, electrostatic potential map, and HOMO-LUMO energy levels are conducted using the DMol3 program package in Materials Studio¹. The exchange and correlation terms were determined using the Generalized Gradient Approximation (GGA) in the form proposed by Perdew, Burke, and Ernzerhof (PBE)². The energy convergence criterion was set to 10^{-5} Hartree.

The adsorption of LA and H₂O on the Zn (002) ,(100) and (101) surfaces are investigated in this work. In the surface adsorption model, a vacuum region of approximately 15 Å is introduced in the Z-direction to eliminate the effects of periodic boundary conditions on the slab model.

The binding energy ($\Delta E_{\text{binding}}$) was calculated by $\Delta E_{\text{binding}} = E_{\text{total}} - (E_1 + E_2)$, where E_{total} , E_1 and E_2 are the energy of the optimized system, one of the structures, and another molecule, respectively.

Molecular dynamics (MD) simulations of the bulk electrolytes were performed using the Amorphous Cells module. To study the self-adsorption behavior of LA molecules, a solid-liquid model was constructed. A unit cell electrolyte model contained 100 Zn²⁺, 100 SO₄²⁻, 1750 H₂O, and 30 LA molecules. After geometry optimization, NVT simulations were conducted at 298.15 K for 1500 ps. The solvation structure of Zn²⁺ ions with and without 0.3M LA was also investigated. A unit cell of the LA/BE model contained 50 Zn²⁺, 50 SO₄²⁻, 1750 H₂O, and 30 LA molecules. The system was first simulated in an NPT ensemble for 500 ps until the unit volume stabilized, followed by an NVT simulation for 1000 ps to achieve equilibrium.

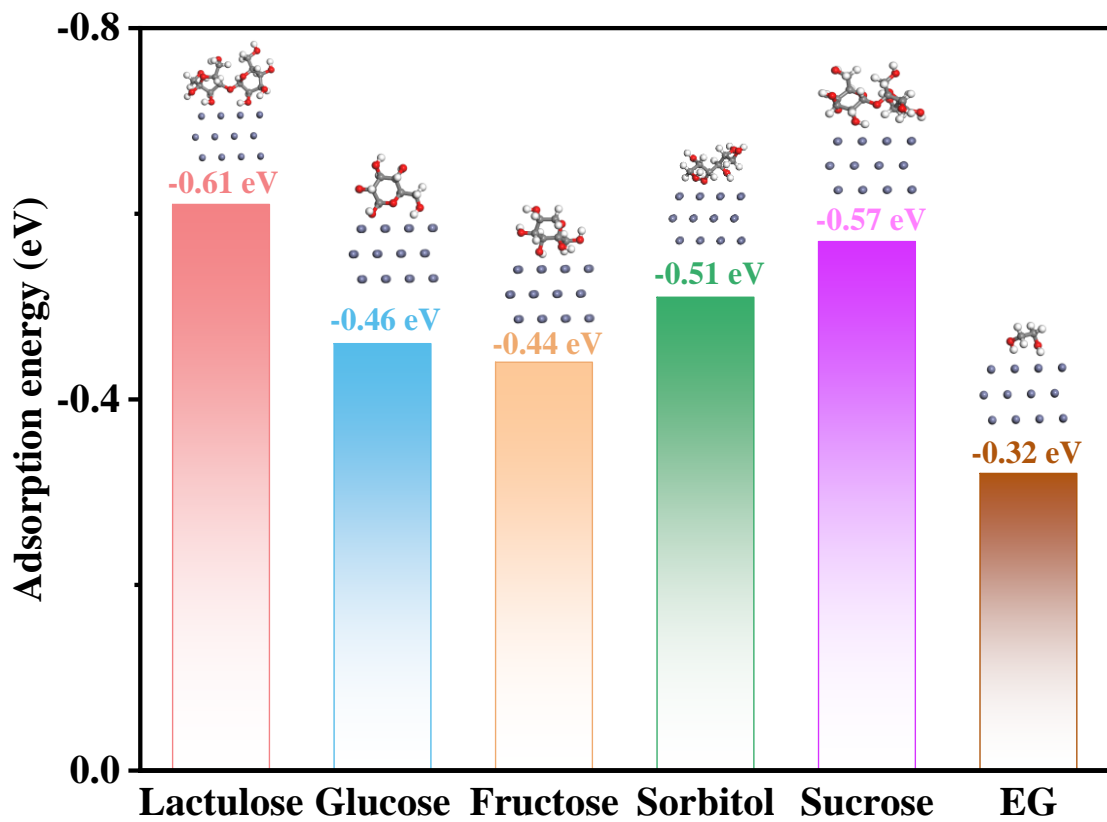


Fig. S1. Adsorption energies of LA and other additives on the Zn(002) surface.

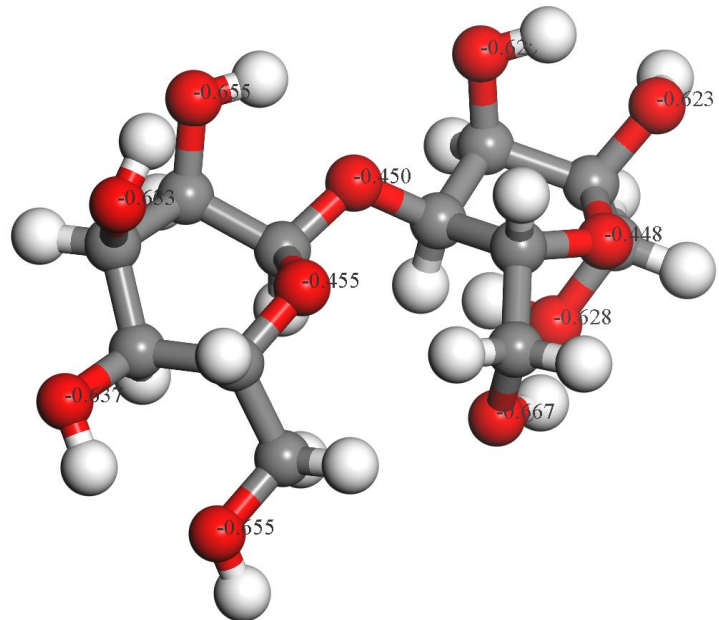


Fig. S2. Mulliken charges of oxygen atoms in LA.

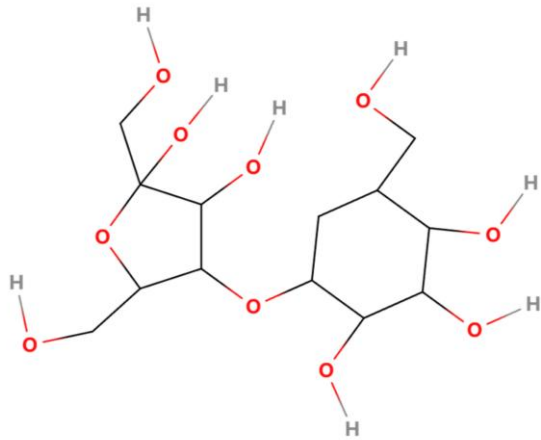


Fig. S3. Molecular structure of Lactulose (LA).

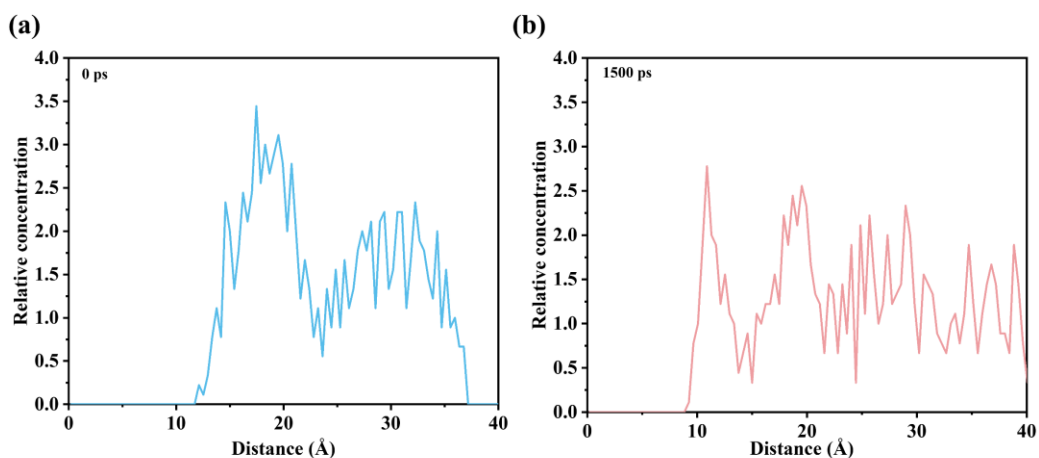


Fig. S4. The relative concentration of LA is distributed at (a) 0 ps, (b) 1500 ps.

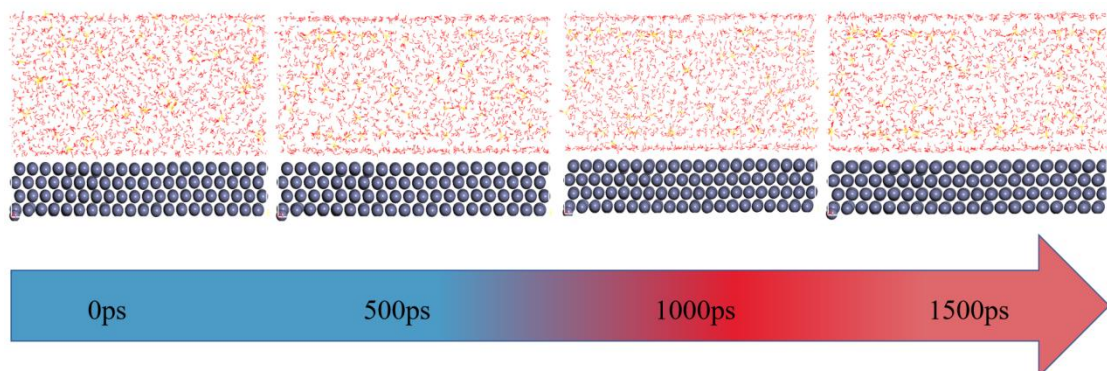


Fig. S5. Snapshots profiles of MD simulations of IHP dynamic formation simulations in the direction perpendicular to Zn surface.

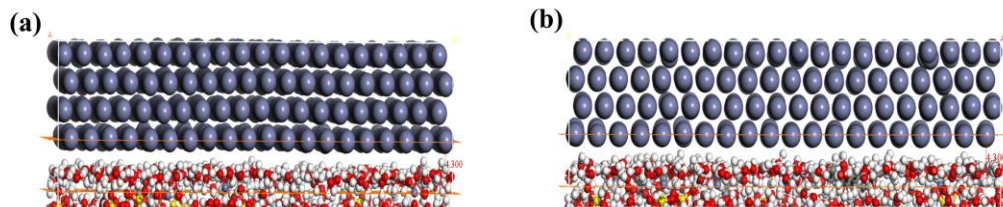


Fig. S6. The interface 4.3 Å from the zinc metal surface: at (a)BE,(b)LA/BE³.

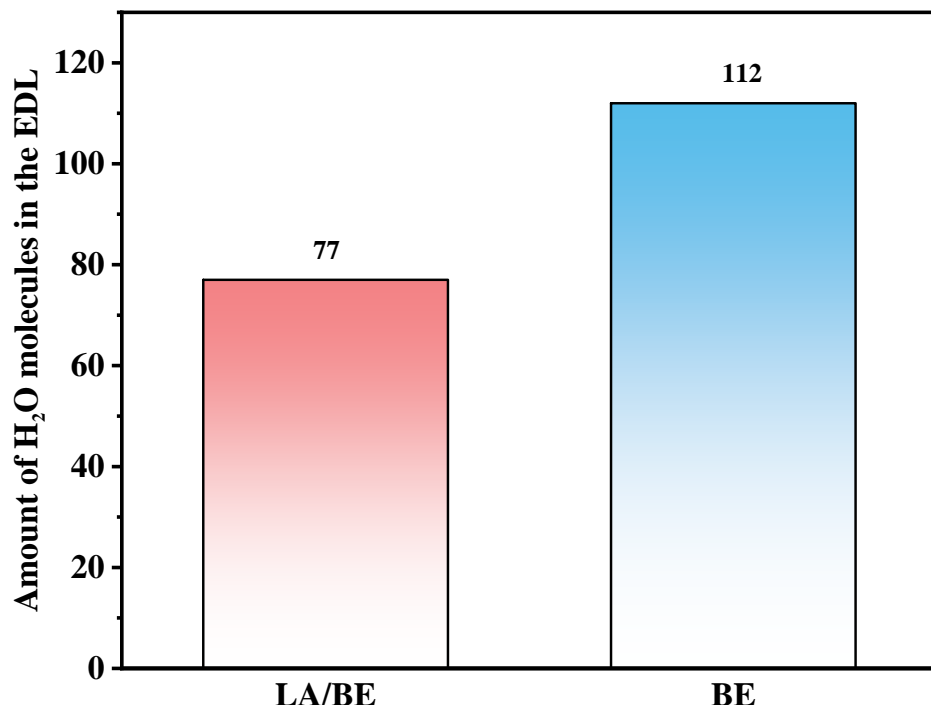


Fig. S7. The number of water molecules within 4.3 Å distance from the surface of zinc metal.

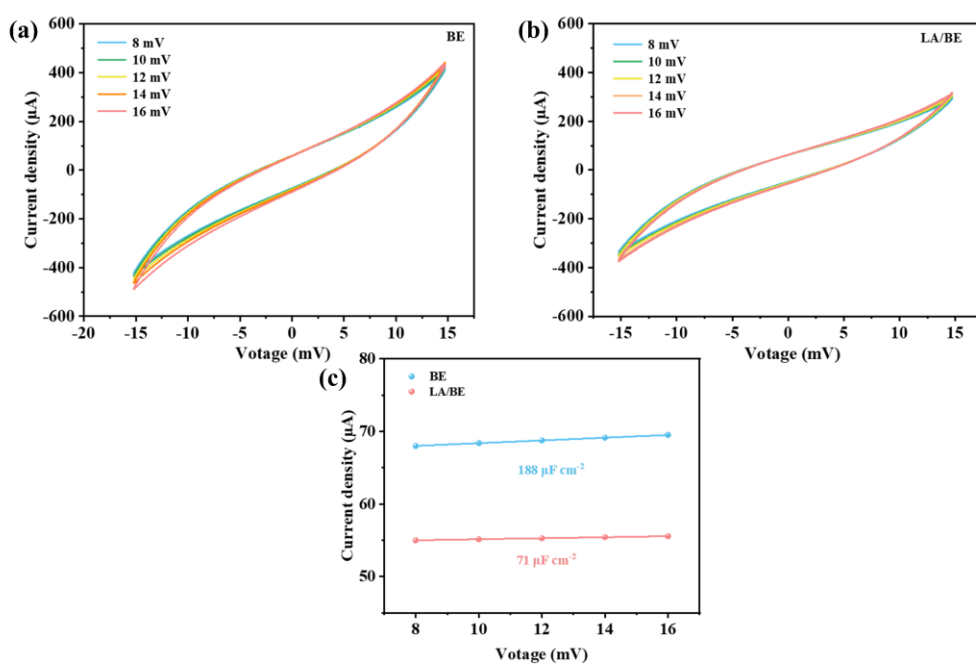


Fig. S8. (a) BE different sweep speed CV (b) LA/BE different sweep speed CV (c) Electric double-layer capacitance (EDLC) curves of BE and LA/BE

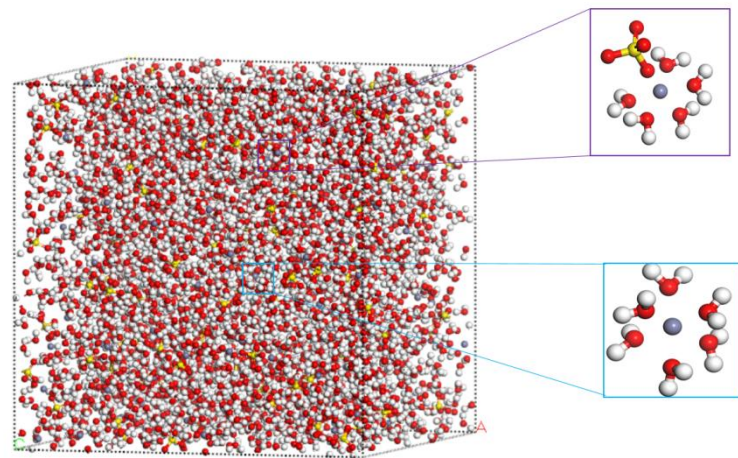


Fig. S9. Snapshot of BE from MD simulations.

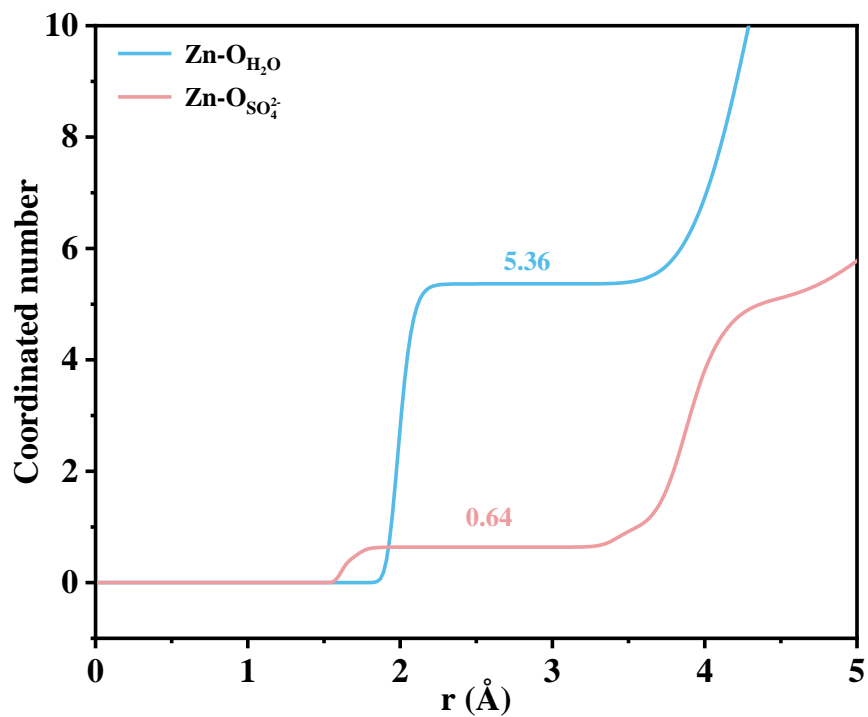


Fig. S10. Coordination number of zinc ions in BE.

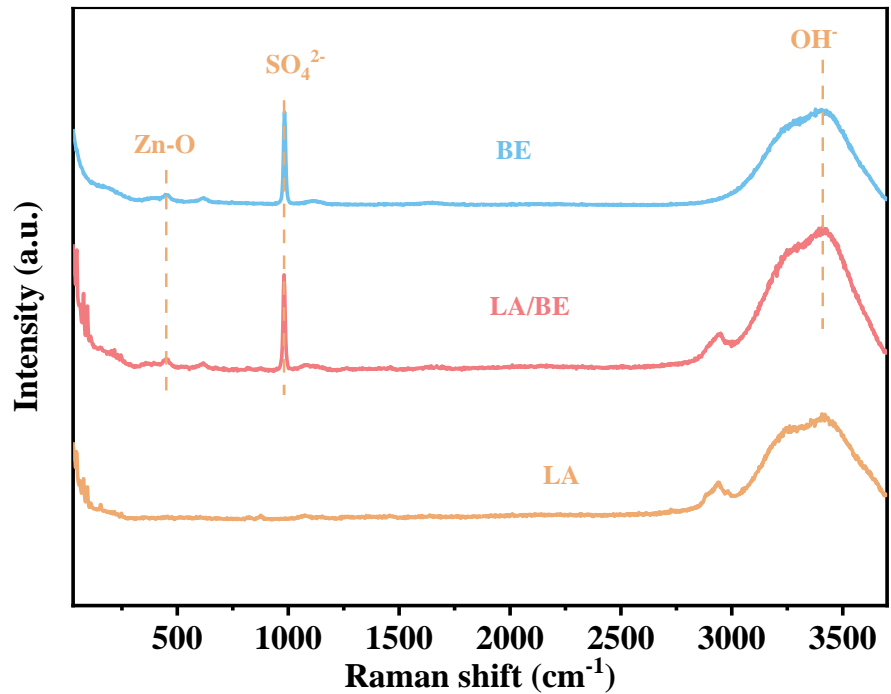


Fig. S11. Raman spectra of BE, LA/BE and LA powder.

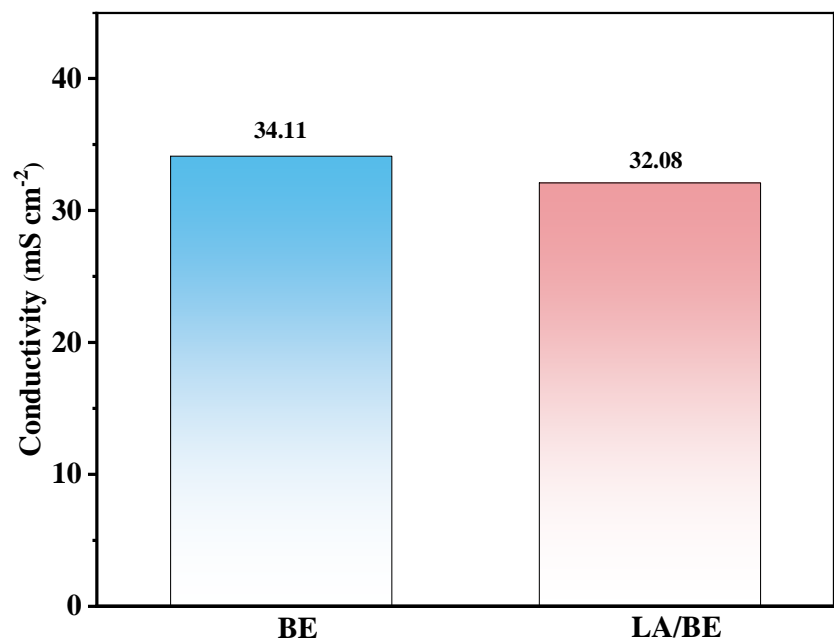


Fig. S12. Ionic conductivity of different electrolytes.



Fig. S13. Digital photos of different concentrations of electrolytes.



Fig. S14. Digital photos of zinc sheets soaked in different concentrations of electrolyte

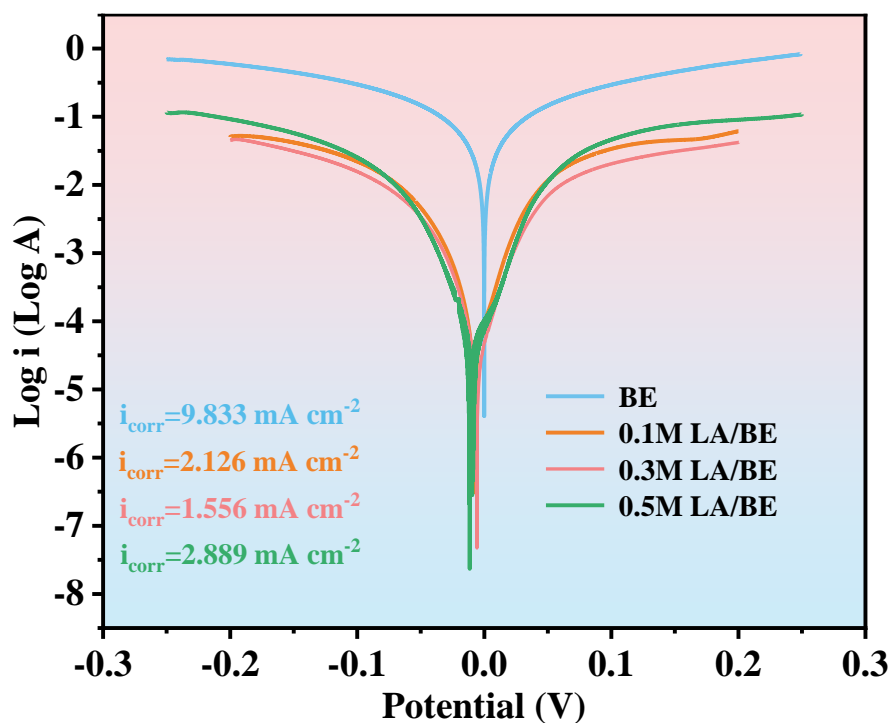


Fig. S15. Tafel curve and corrosion current of electrolyte with different concentration.

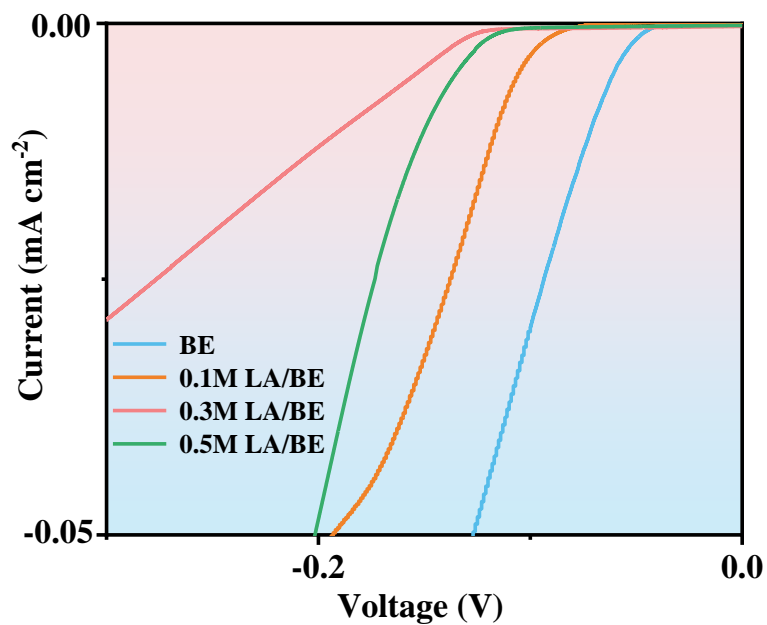


Fig. S16. LSV curve of electrolyte with different concentration.

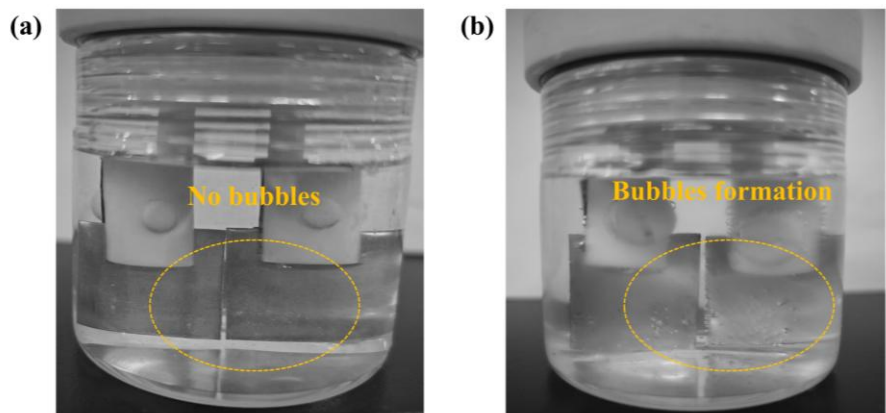


Fig. S17. The transparent battery is charged and discharged in (a)0.3M LA/BE,(b)BE.

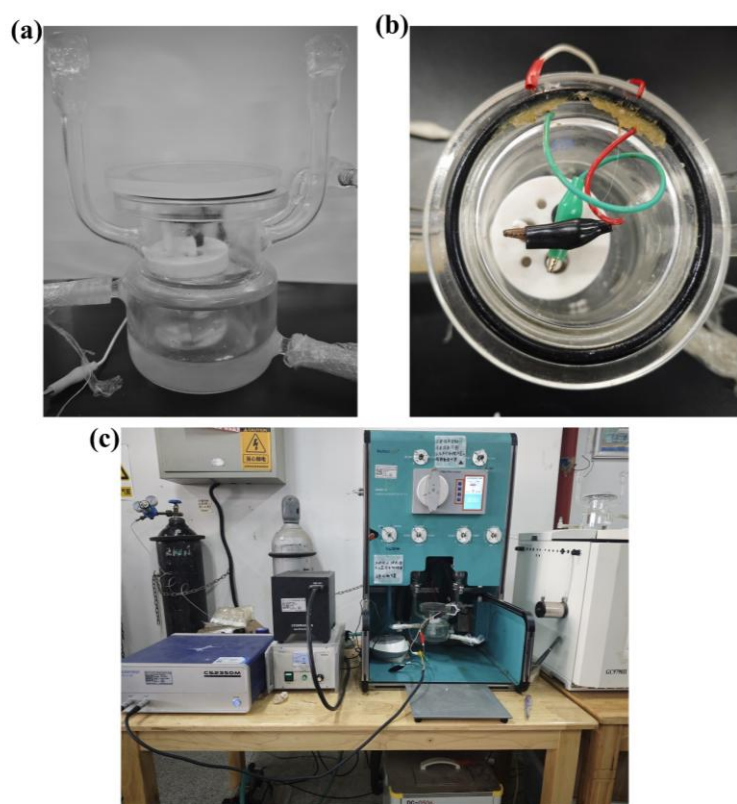


Fig. S18. In situ hydrogen production device.

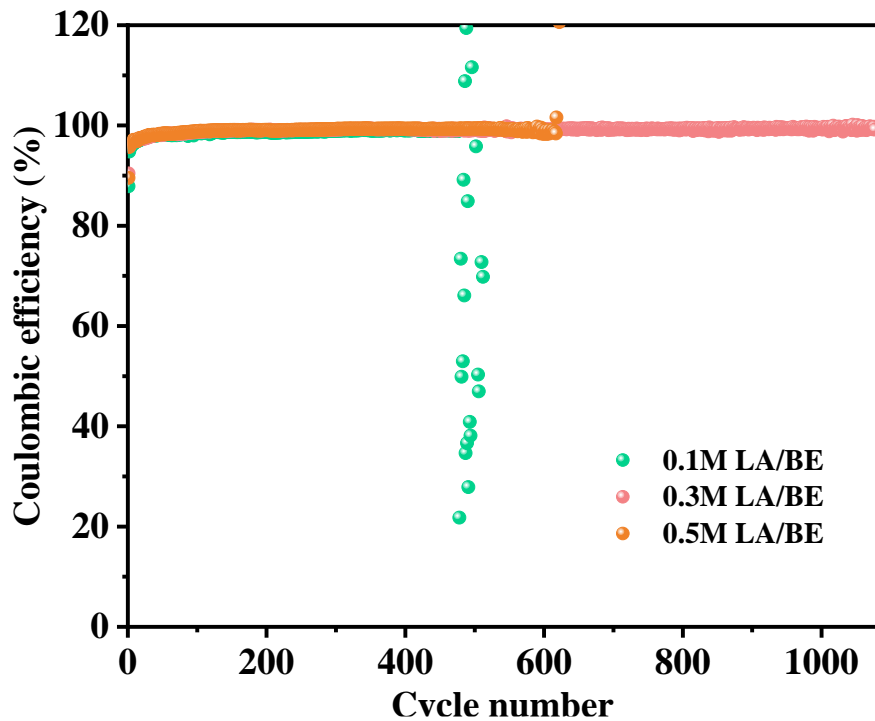


Fig. S19. Coulomb efficiency of Zn||Cu half cells assembled with electrolytes of different concentrations.

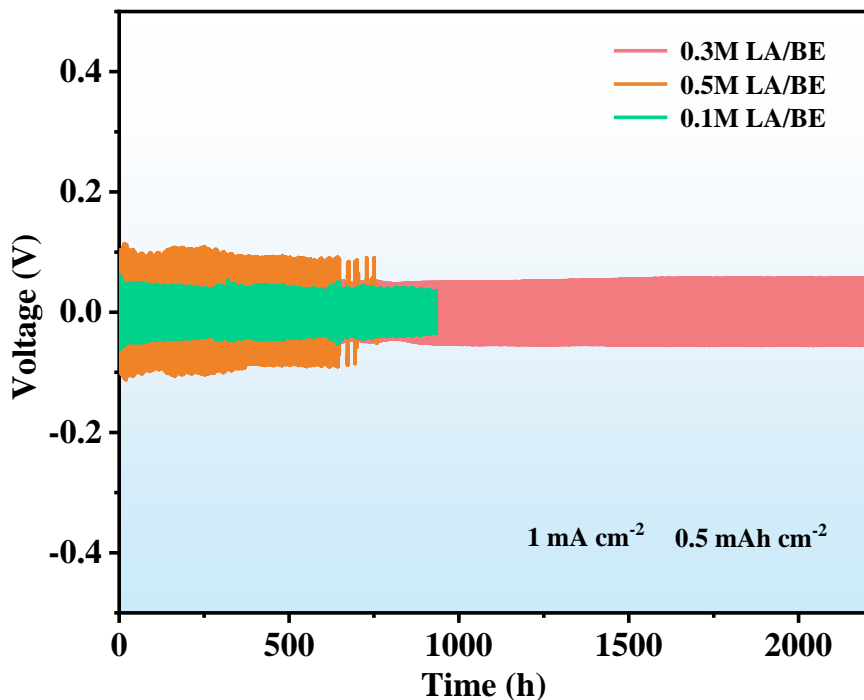


Fig. S20. The Zn||Zn symmetrical battery assembled with different concentrations of electrolyte has a cycle curve of 1 mA cm^{-2} , 0.5 mAh cm^{-2} .

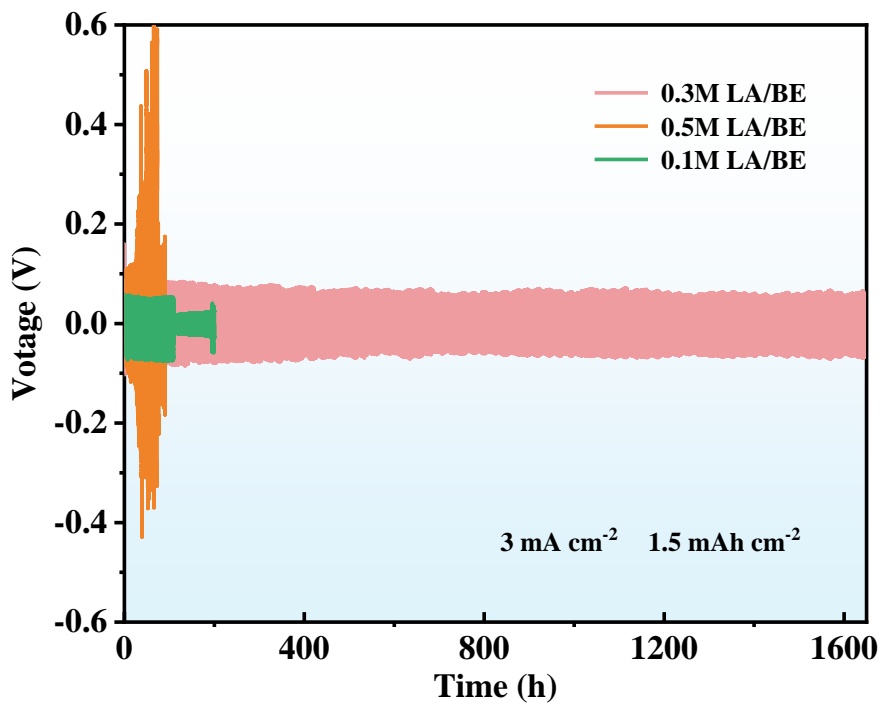


Fig. S21. The Zn||Zn symmetrical battery assembled with different concentrations of electrolyte has a cycle curve of $3 \text{ mA}, 1.5 \text{ mAh}$.

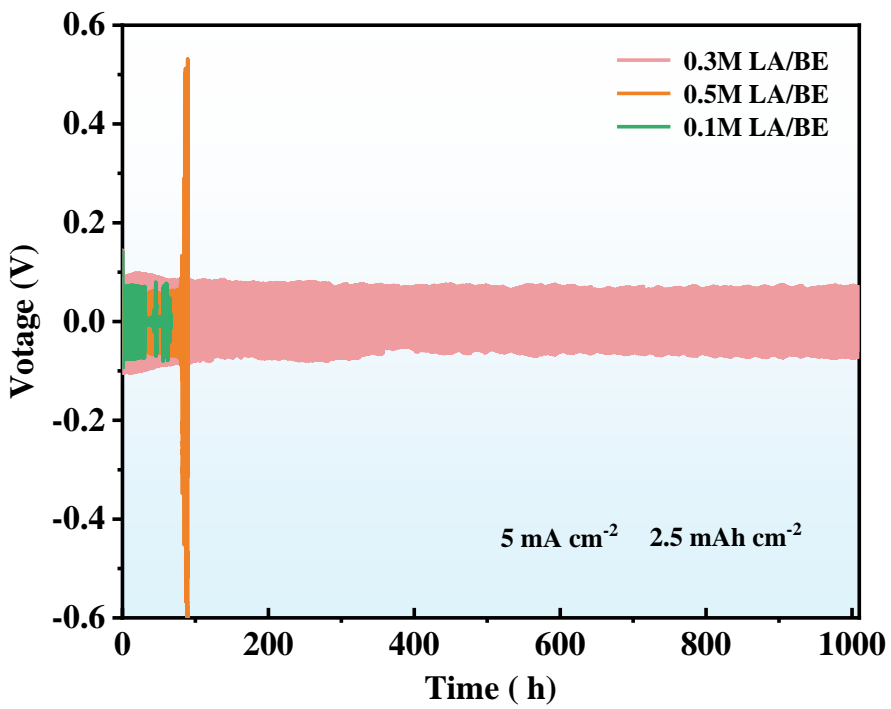


Fig. S22. The Zn||Zn symmetrical battery assembled with different concentrations of electrolyte has a cycle curve of $5 \text{ mA}, 2.5 \text{ mAh}$.

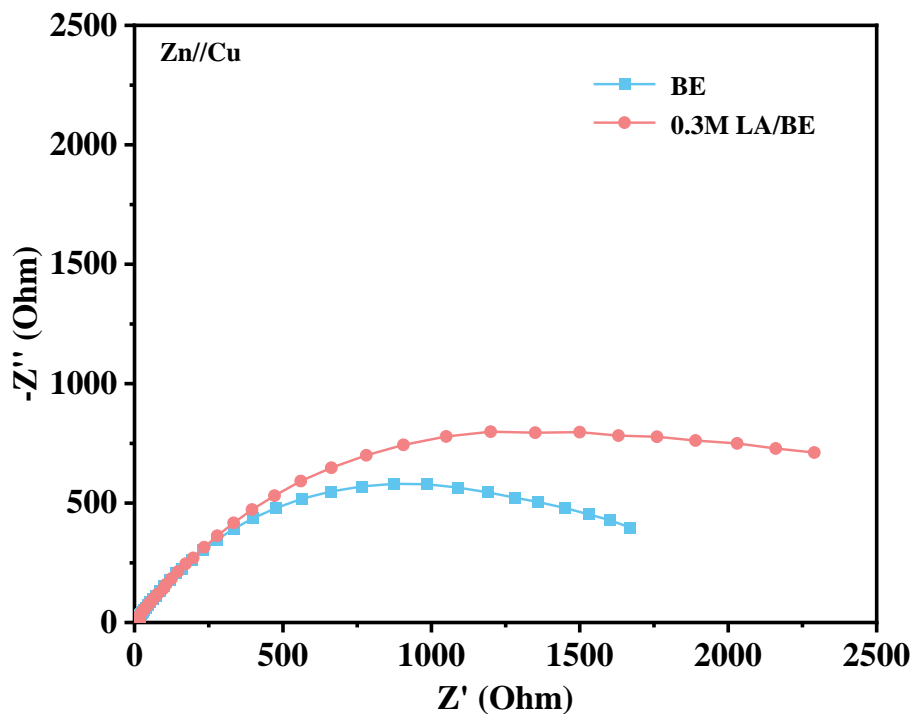


Fig. S23. Impedance of different electrolytes.

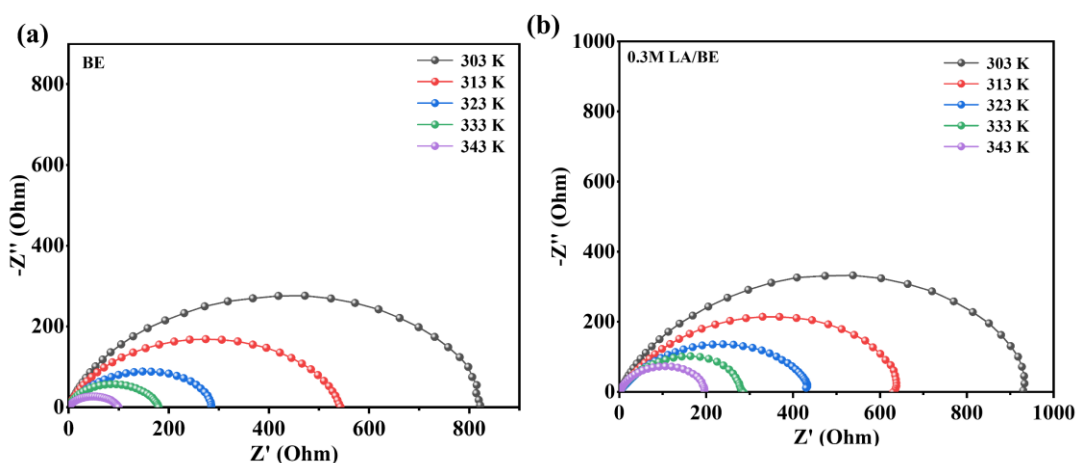


Fig. S24. (a) the impedance of BE at different temperatures, and (b) the impedance of 0.3M LA/BE at different temperatures.

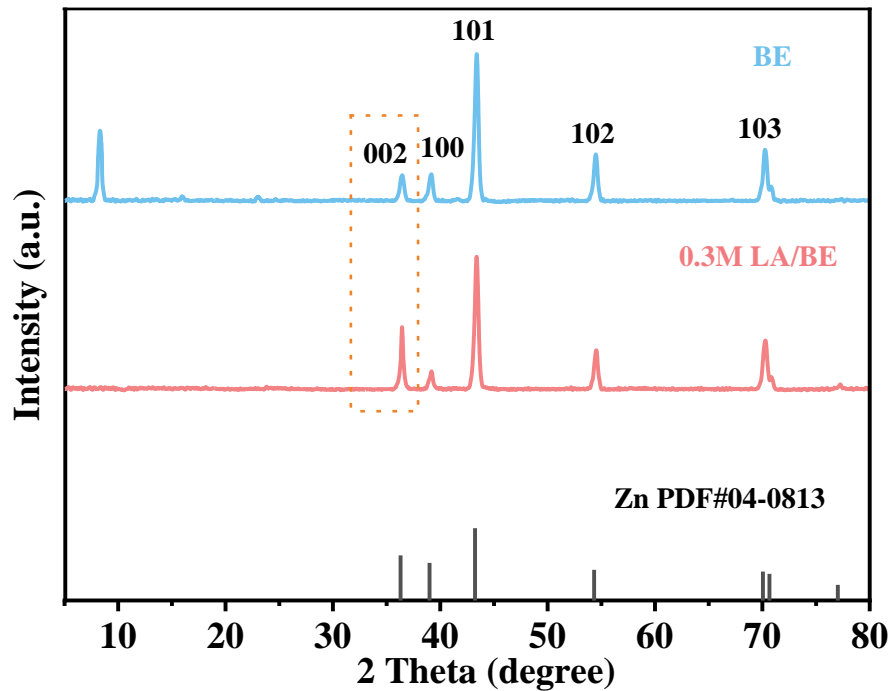


Fig. S25. X-ray diffraction (XRD) patterns of the cycled Zn anode in BE and 0.3M LA/BE electrolytes.

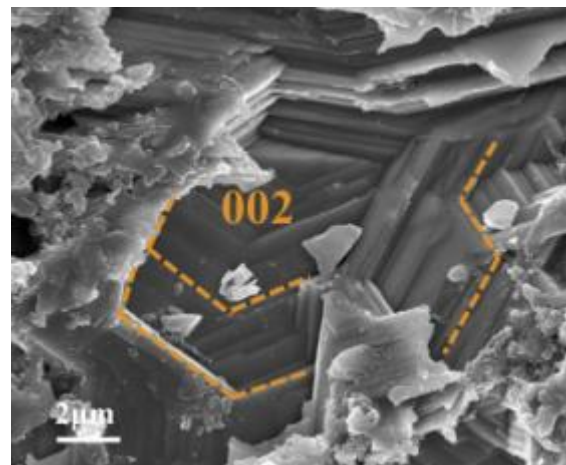


Fig. S26. Scanning electron microscopy (SEM) images of the cycled Zn anode in 0.3M LA/BE electrolyte.

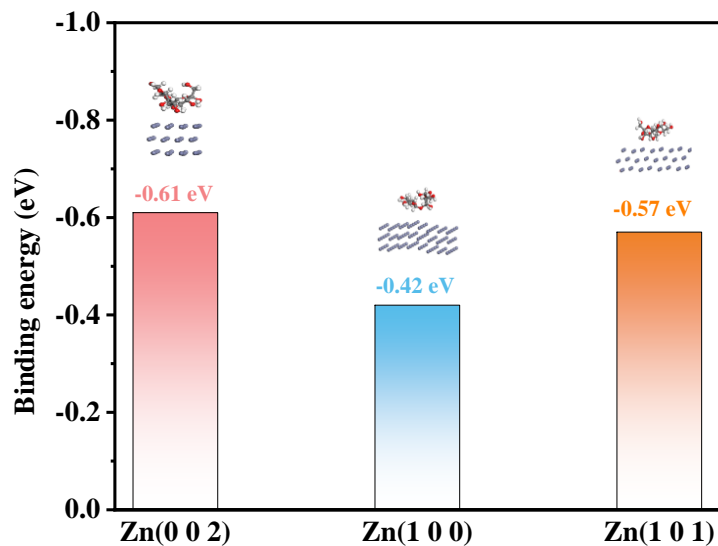


Fig. S27. Adsorption energies of LA molecules on Zn facets, including (002), (100), and (101).

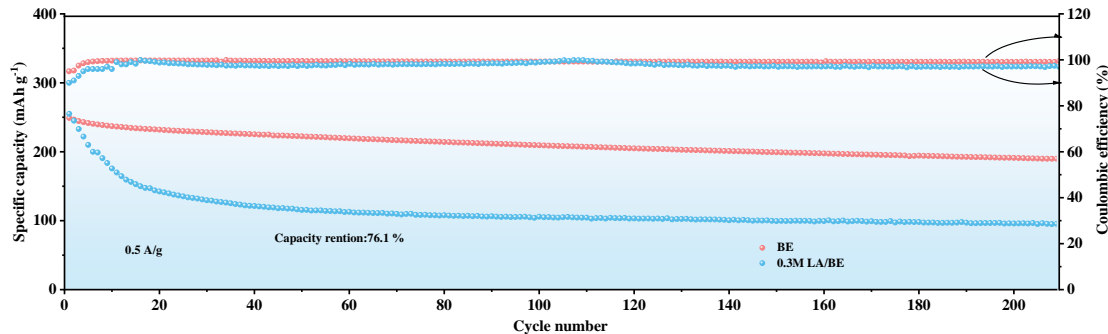


Fig. S28. Comparison of the long-term stability of Zn||MnO₂ full cells under different electrolyte systems at a current density of 0.5 A/g.

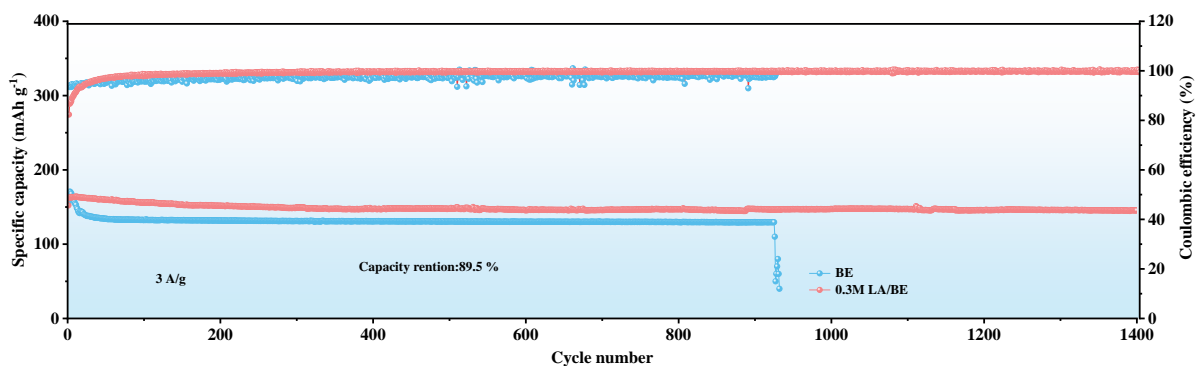


Fig. S29. Comparison of the long-term stability of Zn||MnO₂ full cells under different electrolyte systems at a current density of 3 A/g.

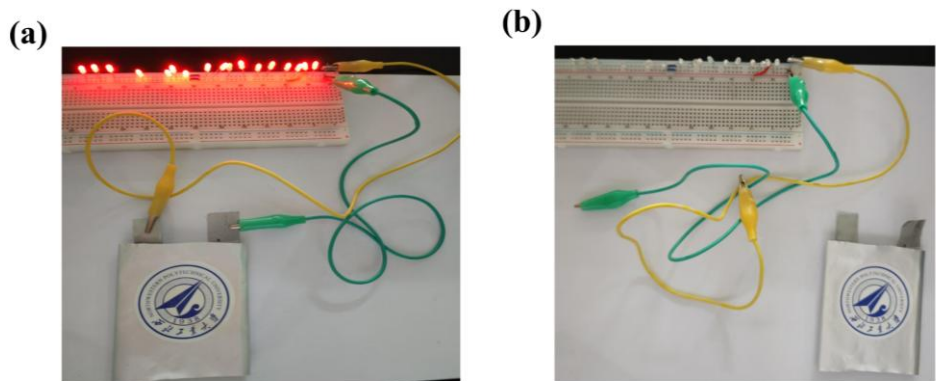


Fig. S30. A digital photo showing an LED light powered by a $\text{Zn}||\text{MnO}_2$ pouch cell.

Table S1 Comparison of cycle life in this work with other literatures based on electrolyte additives.

Electrolyte additive	Current density and capacity	Lifespan	Reference
graphene oxide	1.0 mA cm ⁻² 0.5 mAh cm ⁻²	650 h	⁴
Ce ₂ (SO ₄) ₃	1.0 mA cm ⁻² , 1.0 mAh cm ⁻²	400 h	⁵
SC (Sodium citrate)	1 mA cm ⁻² , 1 mAh cm ⁻²	760 h	⁶
THL (trehalose)	1.0 mA cm ⁻² , 1.0 mAh cm ⁻²	1600 h	⁷
MAAC (methylammonium acetate)	0.5 mA cm ⁻² , 0.5 mAh cm ⁻²	1700 h	⁸
TMB (trifluoro borate)	1.0 mA cm ⁻² , 1.0 mAh cm ⁻²	1800 h	⁹
TEG (triethylene glycol)	1.0 mA cm ⁻² , 1.0 mAh cm ⁻²	2000 h	¹⁰
glucose	1.0 mA cm ⁻² , 1.0 mAh cm ⁻²	2000 h	¹¹
LA (Lactulose)	1.0 mA cm ⁻² , 0.5 mAh cm ⁻²	2200 h	This work

References:

1. L. Cao, D. Li, E. Hu, J. Xu, T. Deng, L. Ma, Y. Wang, X.-Q. Yang and C. Wang, *J. Am. Chem. Soc.*, 2020, **142**, 21404-21409.
2. J. P. Perdew, K. Burke and M. Ernzerhof, *Phys. Rev. Lett.*, 1996, **77**, 3865-3868.
3. K. Fu, T. Liu, M. Xie, Y. Wu, Z. Li, Y. Xin, Y. Liao, C. Liu, H. Huang, D. Ma, F. Zeng and X. Liang, *Adv. Funct. Mater.*, 2024, **34**, 2407895.
4. J. Abdulla, J. Cao, D. Zhang, X. Zhang, C. Sriprachuabwong, S. Kheawhom, P. Wangyao and J. Qin, *ACS Appl. Energy Mater.*, 2021, **4**, 4602-4609.
5. Y. Li, P. Wu, W. Zhong, C. Xie, Y. Xie, Q. Zhang, D. Sun, Y. Tang and H. Wang, *Energy Environ. Sci.*, 2021, **14**, 5563-5571.
6. X. Liu, L. Yue, W. Dong, Y. Qu, X. Sun and L. Chen, *Batteries*, 2024, **10**, 97.
7. H. Li, Y. Ren, Y. Zhu, J. Tian, X. Sun, C. Sheng, P. He, S. Guo and H. Zhou, *Angew. Chem. Int. Ed.*, 2023, **62**, e202310143.
8. L. Zheng, H. Li, X. Wang, Z. Chen, C. Hu, K. Wang, G. Guo, S. Passerini and H. Zhang, *ACS Energy Lett.*, 2023, **8**, 2086-2096.
9. Z. Zha, T. Sun, D. Li, T. Ma, W. Zhang and Z. Tao, *Energy Storage Mater.*, 2024, **64**, 103059.
10. Y. Li, J. Cheng, D. Zhao, X. Chen, G. Sun, S. Qiao, W. Zhang and Q. Zhu, *Energy Storage Mater.*, 2023, **63**, 102997.
11. P. Sun, L. Ma, W. Zhou, M. Qiu, Z. Wang, D. Chao and W. Mai, *Angew. Chem. Int. Ed.*, 2021, **60**, 18247-18255.